Neutrino-pair bremsstrahlung from nucleon-nucleon scattering

Yi Li, M. K. Liou, W. M. Schreiber, and B. F. Gibson

Phys. Rev. C **92**, 015504 — Published 22 July 2015

DOI: 10.1103/PhysRevC.92.015504

Neutrino-Pair Bremsstrahlung from Nucleon-Nucleon Scattering

Yi Li

College of Physics and Technology, Guangxi University,

Nanning, Guangxi 530004, People's Republic of China

M. K. Liou

Department of Physics and Institute for Nuclear Theory,

Brooklyn College of the City University of New York, Brooklyn, New York 11210, USA

W. M. Schreiber

Department of Physics, College of Staten Island of the City University of New York,

Staten Island, New York 10314, USA

B. F. Gibson

Theoretical Division, Los Alamos National Laboratory, Los Alamos, New Mexico 87545, USA

PACS number(s): 12.15.Ji, 13.75.Cs, 24.80.+y, 26.60.-c

Abstract

Background: Neutrino-pair bremsstrahlung processes from nucleon-nucleon scattering $NN\nu\bar{\nu}$ ($nn\nu\bar{\nu}$, $pp\nu\bar{\nu}$, and $np\nu\bar{\nu}$) have recently attracted attention in studies of neutrino emission in neutron stars, because of the implications for the neutron star cooling. The calculated $NN\nu\bar{\nu}$ emissivities within the neutron star environment are relatively insensitive to the two-nucleon dynamical model used in the calculations, but differ significantly from those obtained using an OPE model.

Purpose: We investigate the free $NN\nu\bar{\nu}$ cross sections using a realistic nucleon-nucleon scattering amplitude, comparing the relative sizes of the cross sections for the three processes $nn\nu\bar{\nu}$, $pp\nu\bar{\nu}$, and $np\nu\bar{\nu}$.

Method: We employ a realistic one-boson-exchange (ROBE) model for NN scattering and combine those strong scattering amplitudes with the well-known nucleon weak interaction vertices to construct weak bremsstrahlung amplitudes. Using the resulting $NN\nu\bar{\nu}$ amplitudes we investigate the relative importance of the vector (Γ^{μ}_{V}), axial vector (Γ^{μ}_{A}), and tensor (Γ^{μ}_{T}) terms. The ROBE model bremsstrahlung amplitudes are also used as a two-nucleon dynamical model with which we calculate the cross sections $\frac{d\sigma}{d\omega}$ for $nn\nu\bar{\nu}$, $pp\nu\bar{\nu}$, and $np\nu\bar{\nu}$.

Results: The three free $NN\nu\bar{\nu}$ cross sections $\frac{d\sigma}{d\omega}$ are of similar order of magnitude. Each increases with increasing neutrino-pair energy ω. For the neutrino-pair energy of ω = 1 MeV our $nn\nu\bar{\nu}$ results are in quantitative agreement with those previously reported by Timmermans et al. [Phys. Rev. C 65, 064007 (2002)], who used the leading-order term of the soft-neutrino-

pair bremsstrahlung amplitude to calculate the cross sections. Differences between the $nn\nu\bar{\nu}$ and $pp\nu\bar{\nu}$ cross section are not discernible over the nucleon-nucleon incident energy region considered, due to the complete dominance of the axial vector component of the weak interaction nucleon vertex function Γ^{μ} as demonstrated analytically in Appendix A. The $np\nu\bar{\nu}$ cross section is smaller than either the $nn\nu\bar{\nu}$ or the $pp\nu\bar{\nu}$ cross section for low to moderate values of ω; this characteristic only changes at larger neutrino-pair energies around ω~50 MeV, which is above the low energy region characterized in Appendix B.

Conclusions: The free $NN\nu\bar{\nu}$ cross sections, calculated using a realistic nucleon-nucleon amplitude model, are new except for the $nn\nu\bar{\nu}$ cross section at ω=1 MeV that was first reported by Timmermans et al, and at ω=0.5, 1, 2 MeV by Li et al [Phys. Rev. C80, 035505 (2009)]. The $nn\nu\bar{\nu}$ and $pp\nu\bar{\nu}$ cross sections are virtually identical in magnitude. All three $NN\nu\bar{\nu}$ processes are dominated by the axial vector component of the vertex function Γ^{μ}, with only slight deviations from this behavior being seen in the $np\nu\bar{\nu}$ process at large neutrino-pair energies.

I. Introduction

The implications of neutrino-pair bremsstrahlung from nucleon-nucleon scattering for the cooling of neutron stars has been the subject of several recent studies [1-4]. The free processes

$$n + n \rightarrow n + n + \nu + \bar{\nu}\,, \tag{1}$$

$$p + p \rightarrow p + p + \nu + \bar{\nu}\,, \tag{2}$$

$$n + p \rightarrow n + p + \nu + \bar{\nu}\,, \tag{3}$$

are herein denoted as $nn\nu\bar{\nu}$, $pp\nu\bar{\nu}$, and $np\nu\bar{\nu}$, respectively. A primary purpose of these studies is to investigate the role of the nucleon weak interaction vertices, when combined with realistic nucleon-nucleon amplitudes, in the resulting neutrino-pair bremsstrahlung cross sections in the absence of the complications that arise in neutron star model emissivity calculations due to thermal modifications. Neutron star studies have shown that the cross sections or emissivities are not sensitively dependent on the dynamical nucleon-nucleon model used in the calculation, when a realistic representation of the nucleon-nucleon scattering amplitude is generated by the model employed. This is in contrast, for example, to the situation where a simple one-pion-exchange (OPE) model is used, in which case results for the $NN\nu\bar{\nu}$ process are a factor of 3-5 larger than for more realistic scattering amplitude calculations. (The emissivities using the OPE model were first calculated by Friman and Maxwell [5].)

We have developed a realistic one-boson exchange (ROBE) approach for the investigation of electroweak production processes involving nucleon-nucleon scattering. Photon

bremsstrahlung amplitudes in the ROBE approach have been successfully applied to describe $NN\gamma$ ($pp\gamma$, $np\gamma$, and $nn\gamma$) photon bremsstrahlung processes [6-11]. In the present paper, the ROBE amplitudes are used to investigate the $NN\nu\bar{\nu}$ neutrino-pair bremsstrahlung processes. It is crucial that the ROBE $NN\gamma$ amplitudes, as defined in Refs. [6, 9, 10], obey the soft-photon theorem [12-23]; likewise, the ROBE $NN\nu\bar{\nu}$ amplitudes should be consistent with the soft-neutrino-pair method [1,3]. The ROBE amplitude is a complete (vector and axial vector) relativistic amplitude, which is not expanded in powers of ω but which provides a rigorous model independent result to O(ω^0) for the vector contribution and to O(ω^{-1}) for the axial vector contribution.

In the ROBE approach the $NN\gamma$ and $NN\nu\bar{\nu}$ amplitudes are generated from Horowitz's OBE model [24] for the two-nucleon amplitude, which is an alternative representation of the nucleon-nucleon elastic scattering amplitude. Whereas the standard Goldberger-Grisaru-MacDowell-Wong (GGMW) amplitude is expressed in terms of a set of phase shifts [25], the Horowitz amplitude is expressed in terms of a set of OBE parameters (masses, complex coupling constants, and cutoff parameters). These parameters have been determined by fitting to the Arndt [26] amplitudes directly without iteration of the meson exchanges (the tree approximation). Nucleon-nucleon soft-photon bremsstrahlung calculations using the two-u-two-t special (TuTts) amplitude [21, 27-31] have used the GGMW amplitude as input. The agreement between the theoretical predictions using the ROBE and the soft-photon TuTts amplitudes with both the high-precision Kernfysisch-Versneller-Institute (KVI) $pp\gamma$ cross section data [32-34] and the TRIUMF $pp\gamma$ cross section data [35] provides clear examples of the quantitative nature of the ROBE and soft-photon TuTts approaches to describing pp bremsstrahlung [7, 8].

Details of the ROBE model calculations for $nn\nu\bar{\nu}$ cross sections have been previously presented [11]. Numerical results were quantitatively similar to those obtained in the soft-neutrino-pair treatment of Timmermans et al. [1]. The $nn\nu\bar{\nu}$ results will be extended in the present paper. ROBE model results for the $pp\nu\bar{\nu}$ and $np\nu\bar{\nu}$ cross sections are presented for the first time. The ROBE amplitudes for the respective processes are outlined in Section II. The cross section results and their mutual comparisons are given in Section III, together with associated discussion and analysis. A summary and conclusions are provided in Section IV. An analytic analysis of the axial vector dominance is provided in Appendix A, and the low energy region of the neutrino-pair energy ω, in which our numerical results are valid, is investigated in Appendix B.

II. $NN\nu\bar{\nu}$ Amplitudes

The relevant diagrams for the $nn\nu\bar{\nu}$ process are depicted in Fig. 1, while those for the $pp\nu\bar{\nu}$ process are obtained by the replacement of n with p in the diagrams. Figs. 2(a) and 2(b) show the relevant diagrams for the $np\nu\bar{\nu}$ process. In Fig. 2(a) A^0 represents 10 different neutral mesons (π^0, ρ^0, δ^0, t_1^0, a_1^0, n, σ, ω, t_0, and a_0), while in Fig. 2(b) A^+ represents 5 different charged mesons (π^+, ρ^+, δ^+, t_1^+, and a_1^+). The g's denote the respective complex coupling constants, and the λ^α ($\alpha = 1,2,3,4,5$) represent the 5 Fermi covariants. The Z-boson propagator is approximated as

$$-i\frac{g_{\mu\nu} - q_\mu q_\nu / M_Z^2}{q^2 - M_Z^2} \approx i\frac{1}{M_Z^2} g_{\mu\nu} \tag{4}$$

for the neutrino-pair energy region considered. In the c.m. frame, the expression for the cross section $\frac{d\sigma}{d\omega}$ is given by (see, e.g., Ref. [1])

$$\frac{d\sigma}{d\omega} = 3\times\frac{m^4}{2\sqrt{s\left(s-4m^2\right)}\left(2\pi\right)^8}\frac{16\pi}{3}\frac{G_F^2}{2}\frac{\left|\vec{p}_3\right|}{\sqrt{s}-\omega} \times\frac{1}{4}\sum_{\text{nucleon spins}}\iint\left(M_\mu q^\mu M_\rho^* q^\rho - q^2 M^\mu M_\mu^*\right)d\Omega\left(\vec{p}_3\right)d^3\vec{q} \quad , \tag{5}$$

where m is the nucleon mass, $\vec{p}_3$ is the outgoing nucleon c.m. momentum, $q^\mu = \left(\omega,\vec{q}\right)$ is the neutrino-pair four-momentum, $s = 4\left(m^2+\vec{p}^{\,2}\right)$, $\vec{p}$ is the incident nucleon momentum in the c.m. frame, and the Fermi weak interaction constant is $G_F = 1.166\times10^{-5}$ GeV^{-2}. (The Bjorken-Drell convention for the metric and the γ matrices is used.) The factor of 3 arises from the emission of the three neutrino-pair flavors. For the Z-boson propagator approximation defined in Eq. (4) and a coupling constant $\frac{g}{2\cos\theta_W}$ at each vertex, one finds $\frac{g^2}{4M_Z^2\cos^2\theta_W} = \frac{g^2}{4M_W^2} = 2\frac{G_F}{\sqrt{2}}$.

The amplitude M^μ for the $nn\nu\bar{\nu}$ and $pp\nu\bar{\nu}$ processes has the form

$$
\begin{aligned}
M^{\mu} &\equiv M^{\mu}\left(t_{13}, t_{24}, u_{14}, u_{23}\right) \\
&= \sum_{A^0,\alpha}\Bigg\{\Bigg[\frac{F_{A^0}\left(t_{24}\right)}{\left(p_3+q\right)^2-m^2}\,\overline{u}\left(p_3\right)\Gamma^{\mu}\left(\not{p}_3+\not{q}+m\right)g_{NA^0N}\lambda^{\alpha}u\left(p_1\right)\overline{\mathbf{u}}\left(p_4\right)g_{NA^0N}\lambda_{\alpha}u\left(p_2\right) \\
&\quad+\frac{F_{A^0}\left(t_{13}\right)}{\left(p_4+q\right)^2-m^2}\,\overline{u}\left(p_3\right)g_{NA^0N}\lambda^{\alpha}u\left(p_1\right)\overline{\mathbf{u}}\left(p_4\right)\Gamma^{\mu}\left(\not{p}_4+\not{q}+m\right)g_{NA^0N}\lambda_{\alpha}u\left(p_2\right) \\
&\quad+\frac{F_{A^0}\left(t_{24}\right)}{\left(p_1-q\right)^2-m^2}\,\overline{u}\left(p_3\right)g_{NA^0N}\lambda^{\alpha}\left(\not{p}_1-\not{q}+m\right)\Gamma^{\mu}u\left(p_1\right)\overline{\mathbf{u}}\left(p_4\right)g_{NA^0N}\lambda_{\alpha}u\left(p_2\right) \\
&\quad+\frac{F_{A^0}\left(t_{13}\right)}{\left(p_2-q\right)^2-m^2}\,\overline{u}\left(p_3\right)g_{NA^0N}\lambda^{\alpha}u\left(p_1\right)\overline{\mathbf{u}}\left(p_4\right)g_{NA^0N}\lambda_{\alpha}\left(\not{p}_2-\not{q}+m\right)\Gamma^{\mu}u\left(p_2\right)\Bigg] \\
&\quad-\text{terms}\left(p_3\Leftrightarrow p_4, t_{13}\rightarrow u_{14}, t_{24}\rightarrow u_{23}\right)\Bigg\}.
\end{aligned}
\tag{6}
$$

The form of M^{μ} for the $np\nu\overline{\nu}$ can be obtained from Eq. (6) through multiplication by an overall minus sign for $A^0\ (=(\pi^0,\ \rho^0,\ \delta^0,\ t_1^0,\ a_1^0)$ in the first terms, and by the replacement of A^0 by A^+ (see Fig. 2(b)) and the multiplication by a factor of 2 in the second terms.

In Eq. (6), $t_{ij}=\left(p_i-p_j\right)^2$ $(ij=13,24)$ and $u_{ik}=\left(p_i-p_k\right)^2$ $(ik=14,23)$ are Mandelstam variables. The $F_A\left(t_{ij}\right)$ [$F_A\left(u_{ik}\right)$] represent the other relevant factors (defined in terms of t_{ij} and u_{ik}, the mass of the exchanged meson m_A, and the cutoff parameter Λ_A),

$$
F_A\left(t_{ij}\right)=\frac{-4\pi}{t_{ij}-m_A^2}\frac{1}{\left(1-t_{ij}/\Lambda_A^2\right)^2}\qquad(ij=13,24), \tag{7a}
$$

$$
F_A\left(u_{ik}\right)=F_A\left(t_{ij}\rightarrow u_{ik}, ij=13,24\rightarrow ik=14,23\right). \tag{7b}
$$

The weak interaction nucleon vertex functions Γ^{μ}_{nn} and Γ^{μ}_{pp} arising in Eq. (6) for nn and pp vertices, respectively, are

$$\Gamma^{\mu}_{nn} = -\frac{1}{2}\left(F_1^V + 4\sin^2\theta_W F_1^n\right)\gamma^{\mu} - \frac{1}{2}G_A\gamma^{\mu}\gamma^5 + \frac{i}{2}\left(F_2^V + 4\sin^2\theta_W F_2^n\right)\sigma^{\mu\rho}q_{\rho}, \tag{8a}$$

$$\Gamma^{\mu}_{pp} = \frac{1}{2}\left(F_1^V - 4\sin^2\theta_W F_1^p\right)\gamma^{\mu} + \frac{1}{2}G_A\gamma^{\mu}\gamma^5 - \frac{i}{2}\left(F_2^V - 4\sin^2\theta_W F_2^p\right)\sigma^{\mu\rho}q_{\rho}, \tag{8b}$$

where q^{μ} is the outgoing total four-momentum of the emitted neutrino-pair. In Eqs. (8a) and (8b), Γ^{μ} is the sum of vector (Γ^{μ}_V), axial vector (Γ^{μ}_A), and tensor (Γ^{μ}_T) terms, respectively, i.e.,

$$\Gamma^{\mu} = \Gamma^{\mu}_V + \Gamma^{\mu}_A + \Gamma^{\mu}_T. \tag{9}$$

Here,

$$\Gamma^{\mu}_V = \begin{cases} -\frac{1}{2}\left(F_1^V + 4\sin^2\theta_W F_1^n\right)\gamma^{\mu}, & nn \\ \frac{1}{2}\left(F_1^V - 4\sin^2\theta_W F_1^p\right)\gamma^{\mu}, & pp, \end{cases} \tag{10a}$$

$$\Gamma^{\mu}_A = \begin{cases} -\frac{1}{2}G_A\gamma^{\mu}\gamma^5, & nn \\ \frac{1}{2}G_A\gamma^{\mu}\gamma^5, & pp, \end{cases} \tag{10b}$$

$$\Gamma^{\mu}_T = \begin{cases} \frac{i}{2}\left(F_2^V + 4\sin^2\theta_W F_2^n\right)\sigma^{\mu\rho}q_{\rho}, & nn \\ -\frac{i}{2}\left(F_2^V - 4\sin^2\theta_W F_2^p\right)\sigma^{\mu\rho}q_{\rho}, & pp. \end{cases} \tag{10c}$$

Note that a pseudoscalar term of the form $q^\mu \gamma^5$ has been omitted because it yields a term in the cross section which is proportional to the mass of the neutrino, and thus it is negligible. We utilize $F_1^p = 1$, $F_1^n = 0$, $F_1^V = 1$, $F_2^p = \frac{\kappa_p}{2m}$, $F_2^n = \frac{\kappa_n}{2m}$, $F_2^V = \frac{\kappa_p - \kappa_n}{2m}$, $G_A = -1.257$, the nucleon anomalous magnetic moments $\kappa_p = 1.793$ and $\kappa_n = -1.913$, and $\sin^2 \theta_W = 0.234$ for the Weinberg angle θ_W.

The conserved vector current (CVC) hypothesis, i.e. $q_\mu M_V^\mu = 0$, is satisfied by the amplitude M^μ given in Eq. (6) for the $nn\nu\bar{\nu}$ and $pp\nu\bar{\nu}$ processes. To satisfy CVC for the $np\nu\bar{\nu}$ process, an additional gauge term

$$
\begin{aligned}
M'^{\mu}_{V} = {} & 2(G_V^p - G_V^n)(p_1 + p_3 - p_2 - p_4)^\mu \\
& \sum_{A^+,\alpha} \Bigg[\frac{1}{4\pi} (1 - u_{14} / \Lambda^2_{A^+})(1 - u_{23} / \Lambda^2_{A^+}) F_{A^+}(u_{14}) F_{A^+}(u_{23}) \\
& \qquad + \frac{1}{(\Lambda^2_{A^+} - u_{23})} F_{A^+}(u_{14}) + \frac{1}{(\Lambda^2_{A^+} - u_{14})} F_{A^+}(u_{23}) \Bigg] \\
& \overline{u}(p_4) g_{NA^+N} \lambda^\alpha u(p_1) \overline{u}(p_3) g_{NA^+N} \lambda_\alpha u(p_2)
\end{aligned}
\tag{11}
$$

is included, where G_V^n and G_V^p are the respective factors multiplying γ^μ in Eq. (10a).

To incorporate the partially conserved axial vector current hypothesis (PCAC) in the neutrino bremsstrahlung amplitudes would require including internal terms, those which are related to the corresponding internal terms for the associated pion production process. This procedure would be similar to that outlined in Ref. [1], but it inherently contains the uncertainties associated with the pion production internal terms. To our knowledge, no one has actually

reported results for the neutrino bremsstrahlung processes which include such terms, and we have not done so here.

III. $NN\nu\bar{\nu}$ Results and Discussion

The $\frac{d\sigma}{d\omega}$ cross section results for the $nn\nu\bar{\nu}$, $pp\nu\bar{\nu}$, and $np\nu\bar{\nu}$ processes at various neutrino-pair energies ω, over a wide range of incident nucleon center-of-mass momenta p, are shown in Fig. 3. The figure is terminated on the left at 100 MeV/c, which corresponds to a lab energy of 21.3 MeV. We are hesitant to use the Horowitz parameters at lower momenta. The cross sections were obtained by: 1) inserting the appropriate ROBE amplitudes from Eq. (6) into Eq. (5), and 2) performing the indicated five dimensional integration numerically using Monte Carlo techniques. Results for the $nn\nu\bar{\nu}$ process at ω = 0.5, 1, and 2 MeV were previously published [11], and the ω = 1 MeV results were shown to be in quantitative agreement with those obtained by Timmermans et al. [1] (shown also in Fig. 3), who used the leading-order term of the soft neutrino-pair bremsstrahlung amplitude.

In Fig. 3 the cross section differences between the $nn\nu\bar{\nu}$ and $pp\nu\bar{\nu}$ processes are not discernible. The $np\nu\bar{\nu}$ cross sections are seen to be generally smaller than the identical particle cross sections over the range of p in the figure, the difference decreasing at low and high p values. The difference in the sign of the axial vector term in Γ^{μ}_{nn} of Eq. (8a) as compared with Γ^{μ}_{pp} of Eq. (8b), which is associated with the isotopic spin T_3 dependence of the corresponding neutral current, is correlated with this behavior. Indeed, we verified that were this not the case, the $np\nu\bar{\nu}$ cross section $\frac{d\sigma}{d\omega}$ would be larger than that for the $nn\nu\bar{\nu}$ and $pp\nu\bar{\nu}$ processes. It is

likely that cancellations are occurring between complementary diagrams in Figs. (2a) and (2b) which contain Znn and Zpp vertices, respectively, due to this difference of sign.

A plot similar to Fig. 3, which contains only the axial vector contributions Γ_A^μ of the respective Γ^μ vertex functions given in Eqs. (8a) and (8b), would ***not*** differ discernibly from that of Fig. 3. The complete dominance of the axial vector term in the cross section at these neutrino-pair energies ω has been previously noted for the $nn\nu\bar{\nu}$ process [1, 2], and is found to also be the case for the $pp\nu\bar{\nu}$ and $np\nu\bar{\nu}$ processes.

Table 1 at $p = 250$ MeV/c shows the three cross sections $d\sigma/d\omega$, which would be individually obtained from the vector, the axial vector, and the tensor parts of the vertex function Γ^μ. Table 2 at $p = 250$ MeV/c demonstrates explicitly the axial vector dominance. The reason for this dominance is elucidated in Appendix A; in particular, a coherence in the axial vector amplitudes leads to a significant enhancement. That the axial vector contributions to the $nn\nu\bar{\nu}$ and $pp\nu\bar{\nu}$ cross sections are identical accounts for the equality of the two cross sections in the energy range considered. Examination of Table 2 shows virtually no deviation of this behavior at neutrino-pair energies ω as high as 50 MeV . The axial vector dominance for $np\nu\bar{\nu}$ is seen in Table 2 to be not quite as complete; i.e. there are slight contributions to the cross section associated with other elements in the vertex functions Γ_{nn}^μ and Γ_{pp}^μ expressed in Eqs. (8a) and (8b), respectively. The relative size of these contributions is seen in Table 2 to grow with increasing neutrino-pair energy ω. In contradistinction to the ω results shown in Fig. 3, the $np\nu\bar{\nu}$ cross section at $\omega = 50$ MeV given in Table 2 is larger than the corresponding $nn\nu\bar{\nu}$ and

$ppν\bar{ν}$ cross sections. The calculation was extended to 50 MeV to explore whether vector contributions might reveal themselves; such is largely not the case.

In order to glean information as to the region of ω in which our numerical results are valid (the low energy region), we compare in Appendix B our results at $p = 250$ MeV/c with those obtained in leading order $O(1/\omega)$. The commensurate results differ significantly only for $\omega > 50$ MeV. Because the curves in Fig. 3 are relatively flat over the range of p, this conclusion should hold over the range.

IV. Summary and Conclusions

Free cross sections $\frac{d\sigma}{d\omega}$ for the $nnν\bar{ν}$, $ppν\bar{ν}$, and $npν\bar{ν}$ bremsstrahlung processes have been calculated for representative values of the neutrino-pair energy ω. These cross sections have been calculated over a wide range of the center-of-mass incident-nucleon momentum p using the ROBE model. Results for the $nnν\bar{ν}$ process at $\omega = 1$ MeV were previously found [11] to be in quantitative agreement with those obtained by Timmermans et al. [1] using the leading-order term of the soft neutrino-pair bremsstrahlung amplitude.

The cross sections increase with increasing values of the neutrino-pair energy ω, and are of a similar order of magnitude at a given ω. The $nnν\bar{ν}$ and $ppν\bar{ν}$ cross sections are virtually identical in magnitude for neutrino-pair energies as high as $\omega = 50$ MeV. The $npν\bar{ν}$ cross sections are somewhat smaller at low and moderate neutrino-pair energies, but this behavior is modified at higher values of ω, so that at $\omega = 50$ MeV the $npν\bar{ν}$ cross section exceeds that of $nnν\bar{ν}$ and $ppν\bar{ν}$. The neutrino-pair bremsstrahlung cross sections are completely dominated by

the axial vector component Γ_A^μ of the weak interaction nucleon vertex functions Γ_{nn}^μ and Γ_{pp}^μ, which accounts for the qualitative difference from those of photon bremsstrahlung, where non axial vector terms dominate. The reason for this dominance was investigated in detail in Appendix A. Furthermore, the axial vector dominance allowed us to introduce in Appendix B a method to characterize the low energy region. Small contributions from other elements of the vertex function become evident in the $npv\bar{v}$ cross section at high values of ω.

Acknowledgements

Numerical results in this paper were performed on the supercomputer of the CUNY High Performance Computing Center situated at the College of Staten Island. The work of Y. Li was supported by a grant from Guangxi University, the work of M. K. Liou and W. M. Schreiber was supported in part by the CUNY Professional Staff Congress-Board of Higher Education Research Award Program, and the work of B. F. Gibson was carried out under the auspices of the National Security Administration of the US Department of Energy at Los Alamos National Laboratory under Contract No. DEAC52-06NA25396.

References

[1] R. G. E. Timmermans, A. Y. Korchin, E. N. E. van Dalen, and A. E. L. Dieperink, Phys. Rev. C **65**, 064007 (2002).

[2] E. N. E. van Dalen, A. E. L. Dieperink, and J. A. Tjon, Phys. Rev. C **67**, 065807 (2003).

[3] C. Hanhart, D. R. Phillips, and S. Reddy, Phys. Lett. B **499**, 9 (2001).

[4] S. Stoica, V. P. Paun, and A. G. Negoita, Phys. Rev. C **69**, 068801 (2004).

[5] B. L. Friman, and O. V. Maxwell, The Astrophys. J. **232**, 541 (1979).

[6] M. K. Liou, Y. Li, W. M. Schreiber, and R. W. Brown, Phys. Rev. C **52**, R2346 (1995).

[7] Y. Li, M. K. Liou, and W. M. Schreiber, Phys. Rev. C **72**, 024005 (2005).

[8] Y. Li, M. K. Liou, W. M. Schreiber, and B. F. Gibson, Phys. Rev. C **84**, 034007 (2011).

[9] Y. Li, M. K. Liou, and W. M. Schreiber, Phys. Rev. C **64**, 064002 (2001).

[10] Y. Li, M. K. Liou, and W. M. Schreiber, Phys. Rev. C **57**, 507 (1998).

[11] Y. Li, M. K. Liou, and W. M. Schreiber, Phys. Rev. C **80**, 035505 (2009).

[12] F. E. Low, Phys. Rev. **110**, 974 (1958).

[13] E. M. Nyman, Phys. Rev. **170**, 1628 (1968).

[14] S. L. Adler and Y. Dothan, Phys. Rev. **151**, 1267 (1966).

[15] T. H. Burnett and N. M. Kroll, Phys. Rev. Lett. **20**, 86 (1968).

[16] J. S. Bell and R. van Royen. Jr., Nuovo Cimento A **60**, 62 (1969).

[17] L. S. Brown and R. L. Gobed, Phys. Rev. **173**, 1505 (1968).

[18] H. W. Fearing, Phys. Rev. **C6**, 1136 (1972); Phys. Rev. D **7**, 243 (1973).

[19] R. G. E. Timmermans, B. F. Gibson, Yi Li, and M. K. Liou, Phys. Rev. C **65**, 014001 (2001). An appendix of this reference discusses the soft-photon approximation. See this appendix and references cited therein.

[20] M. K. Liou, D. Lin, and B. F. Gibson, Phys. Rev. C **47**, 973 (1993).

[21] M. K. Liou, R. G. E. Timmermans, and B. F. Gibson, Phys. Rev. C **54**, 1574 (1996).

[22] A. Yu. Korchin and O. Scholten, Nucl. Phys. **A581**, 493 (1995).

[23] H. Feshbach and D. R. Yennie, Nucl. Phys. **31**, 150 (1962).

[24] C. J. Horowitz, Phys. Rev. C **31**, 1340 (1985).

[25] M. L. Goldberger, M. T. Grisaru, S. W. MacDowell, and D. Y. Wong, Phys. Rev. **120**, 2250 (1960).

[26] R. A. Arndt and L. D. Roper, Phys. Rev. C 15, 1002 (1977). In Ref. [24] Horowitz states that he used the VPI and SU Scattering Analysis Interactive Dail-in Program and Data Base of R. A. Arndt and D. Roper. He furthermore states in the paper that he uses the winter 1982 amplitudes for the 200 MeV fits, which we have primarily used in our analysis.

[27] R. G. E. Timmermans, T. D. Penninga, B. F. Gibson, and M. K. Liou, Phys. Rev. C **73**, 034006 (2006).

[28] M. K. Liou, T. D. Penninga, R. G. E. Timmermans, and B. F. Gibson, Phys. Rev. C **69**, 011001(R) (2004).

[29] R. G. E. Timmermans, B. F. Gibson, Y. Li, and M. K. Liou, Phys. Rev. C **65**, 014001 (2001).

[30] Y. Li, M. K. Liou, R. Timmermans, and B. F. Gibson, Phys. Rev. C **58**, R1880 (1998).

[31] M. K. Liou, R. Timmermans, and B. F. Gibson, Phys. Lett. B **345**, 372 (1995).

[32] H. Huisman et al., Phys. Rev. Lett. **83**, 4017 (1999).

[33] H. Huisman et al., Phys. Rev. Lett. B **476**, 9 (2000).

[34] H. Huisman and N. Kalantar-Nayestanaki, Phys. Rev. C **64**, 029801 (2001).

[35] K. Michaelian et al., Phys. Rev. D **41** 2689 (1990).

[36] S. Bacca, K. Hally, C. J. Pethick, and A. Schwenk, Phys. Rev. **C** 80, 032802(R) (2009).

Figure and Table Captions in main text

Fig. 1. Diagrams for the $nn\nu\bar{\nu}$ ($pp\nu\bar{\nu}$) processes.

Fig. 2(a). Neutral-meson exchange diagrams for the $np\nu\bar{\nu}$ process.

Fig. 2(b). Charged-meson exchange diagrams for the $np\nu\bar{\nu}$ process.

Fig. 3. The cross sections $\frac{d\sigma}{d\omega}$ for the $nn\nu\bar{\nu}$ ($pp\nu\bar{\nu}$) and $np\nu\bar{\nu}$ processes as a function of the incident neutrino-pair energies ω of (a) 0.5, (b) 1, (c) 2, and (d) 10 MeV, respectively. The dashed curve corresponds to the $nn\nu\bar{\nu}$ ($pp\nu\bar{\nu}$) processes, and the solid curve corresponds to the $np\nu\bar{\nu}$ processes. Also shown is the soft neutrino-pair bremsstrahlung result for the $nn\nu\bar{\nu}$ process at ω = 1 MeV obtained in Ref. [1].

Table 1. Comparison of the $NN\nu\bar{\nu}$ cross sections calculated from the amplitudes for the separated vector, axial vector and tensor parts of the vertex function Γ^{μ}. The cross sections are evaluated at the incident center-of-mass $p = 250$ MeV/c for neutrino-pair energies $\omega = 1$, 10, 25, and 50 MeV .

Table 2. Comparison of the $NN\nu\bar{\nu}$ cross sections calculated from the amplitudes for both the total amplitude and the axial vector amplitude alone. The cross sections are evaluated at the incident center-of-mass $p = 250$ MeV/c for neutrino-pair energies $\omega = 1$, 10, 25, and 50 MeV .

Table 3. Comparison of the percent deviations D_i $(i = pp, nn, np)$ calculated using Eq. (B2). The percent deviations D_i are evaluated at incident center-of-mass $p = 250$ MeV/c for neutrino-pair energies $\omega = 1, 10, 25, 50, 60$ and 65.3 MeV.

p = 250 MeV c^{-1}

ω (MeV)	$\frac{d\sigma_{nn}(\Gamma^{\mu}_{A})}{d\omega}$ (mb MeV^{-1})	$\frac{d\sigma_{nn}(\Gamma^{\mu}_{V})}{d\omega}$ (mb MeV^{-1})	$\frac{d\sigma_{nn}(\Gamma^{\mu}_{T})}{d\omega}$ (mb MeV^{-1})	$\frac{d\sigma_{pp}(\Gamma^{\mu}_{A})}{d\omega}$ (mb MeV^{-1})	$\frac{d\sigma_{pp}(\Gamma^{\mu}_{V})}{d\omega}$ (mb MeV^{-1})	$\frac{D\varsigma_{pp}(\Gamma^{\mu}_{T})}{d\omega}$ (mb MeV^{-1})	$\frac{d\sigma_{np}(\Gamma^{\mu}_{A})}{d\omega}$ (mb MeV^{-1})	$\frac{d\sigma_{np}(\Gamma^{\mu}_{V})}{d\omega}$ (mb MeV^{-1})	$\frac{d\sigma_{np}(\Gamma^{\mu}_{T})}{d\omega}$ (mb MeV^{-1})
1	9.11×10^{-24}	7.32×10^{-28}	1.24×10^{-30}	9.11×10^{-24}	3.00×10^{-30}	1.41×10^{-30}	4.67×10^{-24}	3.96×10^{-26}	6.99×10^{-31}
10	9.21×10^{-21}	6.83×10^{-25}	1.27×10^{-25}	9.21×10^{-21}	2.80×10^{-27}	1.44×10^{-25}	4.71×10^{-21}	4.08×10^{-23}	7.10×10^{-26}
25	1.40×10^{-19}	1.15×10^{-23}	1.26×10^{-23}	1.40×10^{-19}	4.71×10^{-26}	1.42×10^{-23}	7.72×10^{-20}	8.28×10^{-22}	7.40×10^{-24}
50	7.13×10^{-19}	1.49×10^{-22}	3.47×10^{-22}	7.13×10^{-19}	6.12×10^{-25}	3.89×10^{-22}	8.55×10^{-19}	1.32×10^{-20}	3.41×10^{-22}

Table 1

p = 250 MeV c^{-1}

ω (MeV)	$\frac{d\sigma_{nn}}{d\omega}$ (mb MeV^{-1})	$\frac{d\sigma_{nn}(\Gamma^{\mu}_{A})}{d\omega}$ (mb MeV^{-1})	$\frac{d\sigma_{pp}}{d\omega}$ (mb MeV^{-1})	$\frac{d\sigma_{pp}(\Gamma^{\mu}_{A})}{d\omega}$ (mb MeV^{-1})	$\frac{d\sigma_{np}}{d\omega}$ (mb MeV^{-1})	$\frac{d\sigma_{np}(\Gamma^{\mu}_{A})}{d\omega}$ (mb MeV^{-1})
1	9.10×10^{-24}	9.11×10^{-24}	9.11×10^{-24}	9.11×10^{-24}	4.71×10^{-24}	4.67×10^{-24}
10	9.20×10^{-21}	9.21×10^{-21}	9.21×10^{-21}	9.21×10^{-21}	4.76×10^{-21}	4.71×10^{-21}
25	1.39×10^{-19}	1.40×10^{-19}	1.40×10^{-19}	1.40×10^{-19}	7.78×10^{-20}	7.72×10^{-20}
50	7.12×10^{-19}	7.13×10^{-19}	7.13×10^{-19}	7.13×10^{-19}	8.75×10^{-19}	8.55×10^{-19}

Table 2

p = 250 MeV c^{-1}

ω (MeV)	$ppv\bar{v}$ D_{pp} (%)	$nnv\bar{v}$ D_{nn} (%)	$npv\bar{v}$ D_{np} (%)
1	0.5	0.5	1.5
10	1.0	0.9	2.3
25	1.4	1.4	4.4
50	2.1	2.0	6.2
60	11.2	11.1	20.4
65.3	19.2	19.1	37.4

Table 3

Appendix A. Axial Vector Dominance

We investigate in detail why the respective $NN\nu\bar{\nu}$ processes are dominated by the axial vector part of Γ^{μ}. This dominance of the axial vector part has been noted previously [5]. The axial vector part alone is employed in a recent paper [36] which calculates rates for neutrino processes involving two nucleons using chiral effective field theory. The leading order single-pion exchange is suppressed to higher order. The authors point out that the results obtained are similar to those obtained using a phase shift treatment. The latter has been used previously [3] to calculate neutrino-pair and axion emissivities from nucleon-nucleon scattering.

The amplitudes for the $pp\nu\bar{\nu}$, $nn\nu\bar{\nu}$ and $np\nu\bar{\nu}$ processes can be obtained from Eq. (6). As shown in Eq. (9), the weak interaction nucleon vertex function Γ^{μ} in Eq. (6) contains vector (Γ_V^{μ}), axial vector (Γ_A^{μ}), and tensor (Γ_T^{μ}) terms. By using the following vertex functions,

$$\Gamma_{Vpp}^{\mu} \equiv \Gamma_{Vpp}\gamma^{\mu} = \frac{1}{2}\left(F_1^V - 4\sin^2\theta_w F_1^p\right)\gamma^{\mu}, \tag{A1}$$

$$\Gamma_{Vnn}^{\mu} \equiv \Gamma_{Vnn}\gamma^{\mu} = -\frac{1}{2}\left(F_1^V + 4\sin^2\theta_w F_1^n\right)\gamma^{\mu}, \tag{A2}$$

$$\Gamma_{App}^{\mu} \equiv \Gamma_{App}\gamma^{\mu}\gamma^5 = \frac{1}{2}G_A\gamma^{\mu}\gamma^5, \tag{A3}$$

$$\Gamma_{Ann}^{\mu} \equiv \Gamma_{Ann}\gamma^{\mu}\gamma^5 = -\frac{1}{2}G_A\gamma^{\mu}\gamma^5, \tag{A4}$$

We can define six special amplitudes:

(i) The special amplitude M^{μ}_{Vpp} (or M^{μ}_{Vnn}), which depends only on the vector vertex function, can be obtained from Eq. (6) for the $pp\nu\bar{\nu}$ (or $nn\nu\bar{\nu}$) process if Γ^{μ} in Eq. (6) is replaced by Γ^{μ}_{Vpp} (or Γ^{μ}_{Vnn}).

(ii) The special amplitude M^{μ}_{Vnp}, which depends only on the vector vertex function, can be obtained from Eq. (6) for the $np\nu\bar{\nu}$ process if Γ^{μ} in Eq. (6) is replaced by Γ^{μ}_{Vpp} (when the $\nu\bar{\nu}$-pair is emitted from the proton leg) or Γ^{μ}_{Vnn} (when the $\nu\bar{\nu}$-pair is emitted from the neutron leg).

(iii) The special amplitude M^{μ}_{App} (or M^{μ}_{Ann}), which depends only on the axial vector vertex function, can be obtained from Eq. (6) for the $pp\nu\bar{\nu}$ (or $nn\nu\bar{\nu}$) process if Γ^{μ} in Eq. (6) is replaced by Γ^{μ}_{App} (or Γ^{μ}_{Ann}).

(iv) The special amplitude M^{μ}_{Anp}, which depends only on the axial vector vertex function, can be obtained from Eq. (6) for the $np\nu\bar{\nu}$ process if Γ^{μ} in Eq. (6) is replaced by Γ^{μ}_{App} (when the $\nu\bar{\nu}$-pair is emitted from the proton leg) or Γ^{μ}_{Ann} (then the $\nu\bar{\nu}$-pair is emitted from the neutron leg).

The main purpose of introducing these new amplitudes ($M^{\mu}_{Vpp}, M^{\mu}_{Vnn}, M^{\mu}_{Vnp}, M^{\mu}_{App}, M^{\mu}_{Ann}, M^{\mu}_{Anp}$) is to explain why the calculated $NN\nu\bar{\nu}$ cross sections, using the general vertex function Γ^{μ} given by Eq. (9) for all three different $NN\nu\bar{\nu}$ processes, are dominated by the axial vector component of Γ^{μ}. In order to do this, we have to find the leading terms for each of these new amplitudes. We first expand each amplitude and then regroup the expanded terms in such a way that the leading terms can be identified. Let the $(M^{\mu}_{i})_{I}$ (i=Vpp,

Vnn, Vnp, App, Ann, Anp) be the leading terms of the amplitudes M_i^μ; we find the following expressions for the $(M_i^\mu)_I$:

(1) The leading terms of the amplitude M_{Vpp}^μ can be written as

$$
\begin{aligned}
&(M_{Vpp}^\mu)_I \\
&= \sum_{A^o,\alpha} \Big\{ F_{A^o}(t_{24})(g_{NA^oN})^2 \Gamma_{Vpp} \\
&\quad \times \left[\bar{u}(p_3) \left(\frac{2\lambda^\alpha p_3^\mu}{2p_3\cdot q} - \frac{2\lambda^\alpha p_1^\mu}{2p_1\cdot q} \right) u(p_1) \right] \bar{u}(p_4)\lambda_\alpha u(p_2) \\
&\quad + F_{A^o}(t_{13})(g_{NA^oN})^2 \Gamma_{Vpp} \bar{u}(p_3)\lambda^\alpha u(p_1) \\
&\quad \times \left[\bar{u}(p_4) \left(\frac{2\lambda_\alpha p_4^\mu}{2p_4\cdot q} - \frac{2\lambda_\alpha p_2^\mu}{2p_2\cdot q} \right) u(p_2) \right] \Big\} \\
&- \sum_{A^o,\alpha} \Big\{ F_{A^o}(u_{23})(g_{NA^oN})^2 \Gamma_{Vpp} \\
&\quad \times \left[\bar{u}(p_4) \left(\frac{2\lambda^\alpha p_4^\mu}{2p_4\cdot q} - \frac{2\lambda^\alpha p_1^\mu}{2p_1\cdot q} \right) (p_1) \right] \bar{u}(p_3)\lambda_\alpha u(p_2) \\
&\quad + F_{A^o}(u_{14})(g_{NA^oN})^2 \Gamma_{Vpp} \bar{u}(p_4)\lambda^\alpha u(p_1) \\
&\quad \times \left[\bar{u}(p_3) \left(\frac{2\lambda_\alpha p_3^\mu}{2p_3\cdot q} - \frac{2\lambda_\alpha p_2^\mu}{2p_2\cdot q} \right) u(p_2) \right] \Big\}
\end{aligned}
\qquad \text{(A5)}
$$

The $(M_{Vpp}^\mu)_I$ has been used to calculate the $pp\nu\bar{\nu}$ cross section $d\sigma_{Vpp}^I / d\omega$ at $\omega = 1$ MeV for p=250 MeV/c. The calculated value of $d\sigma_{Vpp}^I / d\omega$ is 3.00×10^{-30} mb/MeV. When we use the complete special amplitude M_{Vpp}^μ to calculate the $pp\nu\bar{\nu}$ cross section, we obtain exactly the same value. [See Table 1 under the heading $d\sigma_{pp}(\Gamma_V^\mu)/d\omega$.] This implies that the contributions from other terms [of order $O(q^0)$] are negligible. Thus, we verify that the $(M_{Vpp}^\mu)_I$ indeed contains the leading terms of the special amplitude M_{Vpp}^μ.

(2) The leading terms of the amplitude M^{μ}_{Vnn} have the same expression as Eq. (A5), except that Γ_{Vpp} is replaced by Γ_{Vnn}. That is, we have

$$(M^{\mu}_{Vnn})_I = \left(\frac{\Gamma_{Vnn}}{\Gamma_{Vpp}}\right)(M^{\mu}_{Vpp})_I \tag{A6}$$

The $nn\nu\bar{\nu}$ cross section $d\sigma^I_{nn}/d\omega$, at $\omega = 1$ MeV for p=250 MeV/c, can be calculated from $(M^{\mu}_{Vnn})_I$. Using $d\sigma^I_{pp}/d\omega = 3.00\times10^{-30}$ mb/MeV, $\Gamma_{Vpp} = 0.032$, and $|\Gamma_{Vnn}| = 0.5$, we find

$$\begin{aligned} & d\sigma^I_{Vnn}/d\omega \\ &= \left(\frac{\Gamma_{Vnn}}{\Gamma_{Vpp}}\right)^2 \times 3.00\times10^{-30} mb/MeV \\ &= \left(\frac{0.5}{0.032}\right)^2 \times 3.00\times10^{-30} mb/MeV \\ &\approx 7.32\times10^{-28} mb/MeV, \end{aligned} \tag{A7}$$

which is the value shown in Table 1 under the heading $d\sigma_{nn}\left(\Gamma^{\mu}_V\right)/d\omega$ (calculated using the special amplitude M^{μ}_{Vnn}).

(3) The leading terms of the amplitude M^{μ}_{Vnp} can be written as

$$
\begin{aligned}
&(M^{\mu}_{Vnp})_I \\
&= -\sum_{A^o,\alpha}\Big\{F_{A^o}(t_{24})(g_{NA^oN})^2\Gamma_{Vnn} \\
&\quad\times\left[\bar{u}(p_3)\left(\frac{2\lambda^{\alpha}p_3^{\mu}}{2p_3\cdot q}-\frac{2\lambda^{\alpha}p_1^{\mu}}{2p_1\cdot q}\right)u(p_1)\right]\bar{u}(p_4)\lambda_{\alpha}u(p_2) \\
&\quad+F_{A^o}(t_{13})(g_{NA^oN})^2\Gamma_{Vpp}\bar{u}(p_3)\lambda^{\alpha}u(p_1) \\
&\quad\times\left[\bar{u}(p_4)\left(\frac{2\lambda_{\alpha}p_4^{\mu}}{2p_4\cdot q}-\frac{2\lambda_{\alpha}p_2^{\mu}}{2p_2\cdot q}\right)u(p_2)\right]\Big\} \\
&-2\sum_{A^+,\alpha}\Big\{F_{A^+}(u_{23})(g_{NA^+N})^2 \\
&\quad\times\left[\bar{u}(p_4)\left(\frac{2\Gamma_{Vpp}\lambda^{\alpha}p_4^{\mu}}{2p_4\cdot q}-\frac{2\Gamma_{Vnn}\lambda^{\alpha}p_1^{\mu}}{2p_1\cdot q}\right)u(p_1)\right]\bar{u}(p_3)\lambda_{\alpha}u(p_2) \\
&\quad+F_{A^+}(u_{14})(g_{NA^+N})^2\bar{u}(p_4)\lambda^{\alpha}u(p_1) \\
&\quad\times\left[\bar{u}(p_3)\left(\frac{2\Gamma_{Vnn}\lambda_{\alpha}p_3^{\mu}}{2p_3\cdot q}-\frac{\Gamma_{Vpp}\lambda_{\alpha}p_2^{\mu}}{2p_2\cdot q}\right)u(p_2)\right]\Big\}
\end{aligned}
\tag{A8}
$$

The $(M^{\mu}_{Vnp})_I$ has been used to calculate the $npv\bar{v}$ cross section $d\sigma^I_{Vnp}/d\omega$ at $\omega=1$ MeV for p=250 MeV/c. The calculated value of $d\sigma^I_{Vnp}/d\omega$ is 3.96×10^{-26} mb/MeV. Using the complete special amplitude M^{μ}_{Vnp}, we have also calculated the $npv\bar{v}$ cross section $d\sigma_{np}\left(\Gamma^{\mu}_V\right)/d\omega$ at $\omega=1$ MeV for p=250 MeV/c. The calculated value of $d\sigma_{np}\left(\Gamma^{\mu}_V\right)/d\omega$ is 3.97×10^{-26} mb/MeV. This value is shown in Table 1 under the heading $d\sigma_{np}\left(\Gamma^{\mu}_V\right)/d\omega$. The difference between the calculated values for $d\sigma^I_{Vnp}/d\omega$ and $d\sigma_{np}\left(\Gamma^{\mu}_V\right)/d\omega$ is extremely small, about 0.2%. Again, we verify that $(M^{\mu}_{Vnp})_I$ contains the leading terms of the special amplitude M^{μ}_{Vnp}.

(4) The leading terms of the special amplitude M^{μ}_{App} can be written as

$$
\begin{aligned}
&(M^{\mu}_{App})_I \\
&= \sum_{A^o,\alpha} \Big\{ F_{A^o}(t_{24}) \Gamma_{App} (g_{NA^oN})^2 \\
&\quad \times \left[-\bar{u}(p_3) \left(\frac{2p_3^{\mu}\gamma^5\lambda^{\alpha}}{2p_3\cdot q} + \frac{2p_1^{\mu}\lambda^{\alpha}\gamma^5}{2p_1\cdot q} \right) u(p_1) \right] \bar{u}(p_4)\lambda_{\alpha} u(p_2) \\
&\quad + F_{A^o}(t_{13}) \Gamma_{App} (g_{NA^oN})^2 \bar{u}(p_3)\lambda^{\alpha} u(p_1) \\
&\quad \times \left[-\bar{u}(p_4) \left(\frac{2p_4^{\mu}\gamma^5\lambda_{\alpha}}{2p_4\cdot q} + \frac{2p_2^{\mu}\lambda_{\alpha}\gamma^5}{2p_2\cdot q} \right) u(p_2) \right] \\
&\quad - F_{A^o}(u_{23}) \Gamma_{App} (g_{NA^oN})^2 \\
&\quad \times \left[-\bar{u}(p_4) \left(\frac{2p_4^{\mu}\gamma^5\lambda^{\alpha}}{2p_4\cdot q} + \frac{2p_1^{\mu}\lambda^{\alpha}\gamma^5}{2p_1\cdot q} \right) u(p_1) \right] \bar{u}(p_3)\lambda_{\alpha} u(p_2) \\
&\quad - F_{A^o}(t_{14}) \Gamma_{App} (g_{NA^oN})^2 \bar{u}(p_4)\lambda^{\alpha} u(p_1) \\
&\quad \times \left[-\bar{u}(p_3) \left(\frac{2p_3^{\mu}\gamma^5\lambda_{\alpha}}{2p_3\cdot q} + \frac{2p_2^{\mu}\lambda_{\alpha}\gamma^5}{2p_2\cdot q} \right) u(p_2) \right] \Big\}
\end{aligned}
\tag{A9}
$$

The $(M^{\mu}_{App})_I$ has been used to calculate the $pp\nu\bar{\nu}$ cross section $d\sigma^I_{App}/d\omega$ at $\omega = 1$ MeV for p=250 MeV/c. The calculated value of $d\sigma^I_{App}/d\omega$ is 9.09×10^{-24} mb/MeV. Using the complete special amplitude M^{μ}_{App}, the calculated $pp\nu\bar{\nu}$ cross section $d\sigma_{pp}\left(\Gamma^{\mu}_{A}\right)/d\omega$ gives a value of 9.11×10^{-24} mb/MeV, which can be seen in Table 1. Because the difference between the calculated value for $d\sigma^I_{App}/d\omega$ and $d\sigma_{pp}\left(\Gamma^{\mu}_{A}\right)/d\omega$ is only about 0.2%, $(M^{\mu}_{App})_I$ indeed contains the leading terms of the special amplitude M^{μ}_{App}.

(5) The leading terms of the special amplitude M^{μ}_{Ann} have the same expression as Eq. (A9), except that Γ_{App} is changed to Γ_{Ann}. That is, we have

$$
(M^{\mu}_{Ann})_I = \left(\frac{\Gamma_{Ann}}{\Gamma_{App}} \right) (M^{\mu}_{App})_I \tag{A10}
$$

The $nn\nu\bar{\nu}$ cross section $d\sigma^I_{Ann}/d\omega$ can be written as

$$\frac{d\sigma^I_{Ann}}{d\omega} = \left(\frac{\Gamma_{Ann}}{\Gamma_{App}}\right)^2 \frac{d\sigma^I_{App}}{d\omega} \tag{A11}$$

Since

$$\Gamma_{Ann} = -\Gamma_{App} = -\frac{1}{2}G \tag{A12}$$

Eq. (11) gives

$$\frac{d\sigma^I_{Ann}}{d\omega} = \frac{d\sigma^I_{App}}{d\omega}\ , \tag{A13}$$

which implies that the $nn\nu\bar{\nu}$ cross section $d\sigma^I_{Ann}/d\omega$ must be identical with the $pp\nu\bar{\nu}$ cross section $d\sigma^I_{App}/d\omega$ for the same values of ω and p.

(6) The leading terms of the amplitude M^{μ}_{Anp} can be written as

$$
\begin{aligned}
&(M^{\mu}_{Anp})_I \\
&= -\sum_{A^o,\alpha}\Big\{F_{A^o}(t_{24})(g_{NA^oN})^2\left(-\frac{1}{2}G\right) \\
&\quad\times\left[-\bar{u}(p_3)\left(\frac{2p_3^{\mu}\gamma^5\lambda^{\alpha}}{2p_3\cdot q}+\frac{2p_1^{\mu}\lambda^{\alpha}\gamma^5}{2p_1\cdot q}\right)u(p_1)\right]\bar{u}(p_4)\lambda_{\alpha}u(p_2) \\
&\quad+F_{A^o}(t_{13})(g_{NA^oN})^2\left(\frac{1}{2}G\right)\bar{u}(p_3)\lambda^{\alpha}u(p_1) \\
&\quad\times\left[-\bar{u}(p_4)\left(\frac{2p_4^{\mu}\gamma^5\lambda_{\alpha}}{2p_4\cdot q}+\frac{2p_2^{\mu}\lambda_{\alpha}\gamma^5}{2p_2\cdot q}\right)u(p_2)\right]\Big\} \\
&-2\sum_{A^+,\alpha}\Big\{F_{A^+}(u_{23})(g_{NA^+N})^2\left(\frac{1}{2}G\right) \\
&\quad\times\left[\bar{u}(p_4)\left(\frac{2m\gamma^{\mu}\gamma^5\lambda^{\alpha}}{2p_4\cdot q}+\frac{2m\lambda^{\alpha}\gamma^{\mu}\gamma^5}{2p_1\cdot q}\right)u(p_1)\right]\bar{u}(p_3)\lambda_{\alpha}u(p_2) \\
&\quad+F_{A^+}(u_{14})(g_{NA^+N})^2\left(-\frac{1}{2}G\right)\bar{u}(p_4)\lambda^{\alpha}u(p_1) \\
&\quad\times\left[\bar{u}(p_3)\left(\frac{2m\gamma^{\mu}\gamma^5\lambda_{\alpha}}{2p_3\cdot q}+\frac{2m\lambda_{\alpha}\gamma^{\mu}\gamma^5}{2p_2\cdot q}\right)u(p_2)\right]\Big\}
\end{aligned}
\tag{A14}
$$

The $(M^{\mu}_{Anp})_I$ has been used to calculate the $npv\bar{v}$ cross section $d\sigma^I_{Anp}/d\omega$ at $\omega = 1$ MeV for p=250 MeV/c. The calculated value of $d\sigma^I_{Anp}/d\omega$ is 4.66×10^{-24} mb/MeV. Using the complete special amplitude M^{μ}_{Anp}, the value of the calculated $npv\bar{v}$ cross section $d\sigma_{np}\left(\Gamma^{\mu}_{A}\right)/d\omega$ is 4.67×10^{-24} mb/MeV, which can be seen in Table 1. Because the difference between the values for $d\sigma^I_{Anp}/d\omega$ and $d\sigma_{np}\left(\Gamma^{\mu}_{A}\right)/d\omega$ is extremely small, about 0.2%, $(M^{\mu}_{Anp})_I$ indeed contains the leading terms of the amplitude M^{μ}_{Anp}.

Now, we utilize all six $(M^{\mu}_{i})_I$ [$(M^{\mu}_{Vpp})_I$ Eq. (A5), $(M^{\mu}_{Vnn})_I$ Eq. (A6), $(M^{\mu}_{Vnp})_I$ Eq. (A8), $(M^{\mu}_{App})_I$ Eq. (A9), $(M^{\mu}_{Ann})_I$ Eq. (A10) or Eq. (A13), $(M^{\mu}_{Anp})_I$ Eq. A(14)] to explain why the

axial vector contribution is so dominant. Before getting into a more complicated realistic situation, let us first discuss a simple property, which has already been used (and tested) to identify the six leading $(M_i^\mu)_I$. Suppose we consider the following two amplitudes

$$M_{Vij}^\mu = \bar{u}(p_i)\left(M_{Vi}^\mu - M_{Vj}^\mu\right)u(p_j), \tag{A15}$$

$$M_{Aij}^\mu = \bar{u}(p_i)\left(M_{Ai}^\mu + M_{Aj}^\mu\right)u(p_j) \tag{A16}$$

where

$$M_{Vi}^\mu = M_i^\mu \lambda^\alpha, \qquad M_{Ai}^\mu = M_i^\mu \gamma^5 \lambda^\alpha,$$

$$M_{Vj}^\mu = M_j^\mu \lambda^\alpha, \qquad M_{Aj}^\mu = M_j^\mu \gamma^5 \lambda^\alpha.$$

A key difference between these two amplitudes is that the amplitude M_{Vij}^μ in Eq. (A15) involves a "minus" sign between M_{Vi}^μ and M_{Vj}^μ while the amplitude M_{Aij}^μ in Eq. (A16) involves a "plus" sign between M_{Ai}^μ and M_{Aj}^μ. The "plus" sign in Eq. (A16) implies that M_{Ai}^μ and M_{Aj}^μ add coherently to enhance the cross section. We shall call this kind of amplitude the plus-type amplitude. On the other hand, the "minus" sign in Eq. (A15) implies that there is a cancellation between M_{Vi}^μ and M_{Vj}^μ to reduce the cross section. We shall call this kind of amplitude the minus-type amplitude. Observing this simple property in examining all six $(M_i^\mu)_I$, the reason why the axial vector vertex contribution is dominant can be ascertained. Some important results can be summarized as follows:

(i) For the $pp\nu\bar{\nu}$ case, we compare the leading $(M^{\mu}_{Vpp})_I$ [Eq. (A5)] with the leading $(M^{\mu}_{App})_I$ [Eq. (A9)]. (a) From Eq. (A5), we find that the $(M^{\mu}_{Vpp})_I$ involves four minus-type amplitudes inside the four square brackets of Eq. (A5). The cancellation effects reduce the cross section calculated from $(M^{\mu}_{Vpp})_I$. (b) From Eq. (A9), we find that $(M^{\mu}_{App})_I$ involves four plus-type of amplitudes inside four square brackets of Eq. (A9). The combination of the plus-type amplitudes greatly enhances the cross section calculated from $(M^{\mu}_{App})_I$. (c) It is easy to see from Eq. (A5) that $(M^{\mu}_{Vpp})_I$ includes an overall factor of Γ_{Vpp}. On the other hand, from Eq. (A9), the amplitude $(M^{\mu}_{App})_I$ includes an overall factor of Γ_{App}. Because $\Gamma_{Vpp} = 0.032$ and $\Gamma_{App} = 0.629$, we have $\left(\Gamma_{App} / \Gamma_{Vpp}\right) \approx 386$. This indicates that if we judge just from these overall factors alone and ignore all other important aspects, the cross section $d\sigma^I_{App} / d\omega$ [calculated from $(M^{\mu}_{App})_I$] would be 386 times greater than the cross section $d\sigma^I_{Vpp} / d\omega$ [calculated from $(M^{\mu}_{Vpp})_I$]. (d) Combining all results obtained in (a), (b), and (c), we can conclude that (at $\omega = 1$ MeV for p=250 MeV/c)

$$d\sigma^I_{Vpp} / d\omega << d\sigma^I_{App} / d\omega, \tag{A17}$$

which implies that

$$d\sigma_{pp}\left(\Gamma^{\mu}_{V}\right) / d\omega << d\sigma_{pp}\left(\Gamma^{\mu}_{A}\right) / d\omega \tag{A18}$$

As shown in Table 1, this is indeed the case!

(ii) For the $nn\nu\bar{\nu}$ case, we have to compare the amplitude $(M^{\mu}_{Vnn})_I$ [Eq. (A6)] with the amplitude $(M^{\mu}_{Ann})_I$ [Eq. (A10)]. Because the $nn\nu\bar{\nu}$ process is very similar to the $pp\nu\bar{\nu}$ process, we also have $(M^{\mu}_{Vnn})_I$, which involves four minus-type amplitudes, and $(M^{\mu}_{Ann})_I$, which involves four plus-type amplitudes. This implies that the cancellation effect will reduce the cross section $d\sigma^I_{Vnn}/d\omega$ calculated from $(M^{\mu}_{Vnn})_I$ and the coherent addition will enhance the cross section $d\sigma^I_{Ann}/d\omega$ calculated from $(M^{\mu}_{Ann})_I$. This explains why the cross section $d\sigma^I_{Ann}/d\omega$ must be greater than the cross section $d\sigma^I_{Vnn}/d\omega$. However, there is an important difference between the $pp\nu\bar{\nu}$ process and the $nn\nu\bar{\nu}$ process. We have already pointed out that $\Gamma_{Vpp}=0.032$ for the $pp\nu\bar{\nu}$ process while $\Gamma_{Vnn}=-0.5$ for the $nn\nu\bar{\nu}$ process. This difference explains, as shown in Eq. (A7), that $d\sigma^I_{Vnn}/d\omega$ is greater than $d\sigma^I_{Vpp}/d\omega$. Thus, we have demonstrated that the results (Table 1),

$$d\sigma_{nn}\left(\Gamma^{\mu}_{A}\right)/d\omega >> d\sigma_{nn}\left(\Gamma^{\mu}_{V}\right)/d\omega > d\sigma_{pp}\left(\Gamma^{\mu}_{V}\right)/d\omega, \tag{A19}$$

can be understood.

For the $np\nu\bar{\nu}$ case, we compare $(M^{\mu}_{Vnp})_I$ [Eq. (A8)] with $(M^{\mu}_{Anp})_I$ [Eq. A14]]. This $np\nu\bar{\nu}$ case is more complicated than the $pp\nu\bar{\nu}$ [or the Appendix A (iii)] case for the following reasons:

(1) The $(M^{\mu}_{Anp})_I$ given by Eq. (A14) involves two different kinds of plus-type amplitudes. Both of them are defined by Eq. (A16), but they have different expressions for M^{μ}_{Ai} and M^{μ}_{Aj}.

(a) The first kind of plus-type amplitude involves the following expressions for M^{μ}_{Ai} (i=3 or 4) and M^{μ}_{Aj} (j=1 or 2):

$$M^{\mu}_{Ai} = \left(2p_i^{\mu}\gamma^5\lambda^{\alpha}\right)/\left(2p_i\cdot q\right) \qquad \text{(i=3 or 4),} \tag{A20}$$

$$M^{\mu}_{Aj} = \left(2p_j^{\mu}\lambda^{\alpha}\gamma^5\right)/\left(2p_j\cdot q\right) \qquad \text{(j=1 or 2).} \tag{A21}$$

(b) The second kind of plus-type amplitude involves the following expressions for M^{μ}_{Ai} (i=3 or 4) and M^{μ}_{Aj} (j=1 or 2):

$$M^{\mu}_{Ai} = \left(2m\gamma^{\mu}\gamma^5\lambda^{\alpha}\right)/\left(2p_i\cdot q\right) \qquad \text{(i=3 or 4),} \tag{A22}$$

$$M^{\mu}_{Aj} = \left(2m\lambda^{\alpha}\gamma^{\mu}\gamma^5\right)/\left(2p_j\cdot q\right) \qquad \text{(j=1 or 2).} \tag{A23}$$

Because both kinds of plus-type amplitude add M^{μ}_{Ai} and M^{μ}_{Aj} coherently, they will enhance the cross section $d\sigma^{I}_{Anp}/d\omega$ calculated from $(M^{\mu}_{Anp})_I$.

(2) The $(M^{\mu}_{Vnp})_I$ given by Eq (A8) involves two different types of amplitudes: two minus-type amplitudes and two plus-type amplitudes. The first two amplitudes [inside the first two square brackets of Eq. (A8)] belong to the minus-type class. The last two amplitudes [inside the last two square brackets of Eq. (A8)] belong to the plus-type class. Let us explain why the last two amplitudes belong to the plus-type class. Using $\Gamma_{Vpp} = 0.032$ and $\Gamma_{Vnn} = -0.5$, we find

$$\bar{u}(p_4)\left(\frac{2\Gamma_{Vpp}p_4^{\mu}\lambda^{\alpha}}{2p_4\cdot q} - \frac{2\Gamma_{Vnn}p_1^{\mu}\lambda^{\alpha}}{2p_1\cdot q}\right)u(p_1)$$

$$= \bar{u}(p_4)\left(\frac{0.064p_4^{\mu}\lambda^{\alpha}}{2p_4\cdot q} + \frac{p_1^{\mu}\lambda^{\alpha}}{2p_1\cdot q}\right)u(p_1), \tag{A24}$$

$$\bar{u}(p_3)\left(\frac{2\Gamma_{Vnn}p_3^{\mu}\lambda_{\alpha}}{2p_3\cdot q}-\frac{\Gamma_{VPP}p_2^{\mu}\lambda_{\alpha}}{2p_2\cdot q}\right)u(p_2)$$

$$=-\bar{u}(p_3)\left(\frac{p_3^{\mu}\lambda_{\alpha}}{2p_3\cdot q}+\frac{0.064p_2^{\mu}\lambda_{\alpha}}{2p_2\cdot q}\right)u(p_2)\,. \tag{A25}$$

We can see that there are two terms in the amplitude given by Eq. (A24) and also in the amplitude given by Eq. (A25). Because those two terms are connected by a "plus" sign in each amplitude, both amplitudes given by Eqs. (A24) and (A25) are classified as the plus-type. This implies that the two terms in each amplitude will add coherently to enhance cross section $d\sigma_{VnP}^{I}/d\omega$ calculated from $(M_{VnP}^{\mu})_I$. We should also point out that we do not expect the term with a factor of 0.064 to make a significant contribution to the cross section $d\sigma_{Vnp}^{I}/d\omega$.

Combining all results obtained in (1) and (2), we can explain why

$$d\sigma_{Anp}^{I}/d\omega > d\sigma_{Vnp}^{I}/d\omega > d\sigma_{Vnn}^{I}/d\omega, \tag{A26}$$

and also

$$d\sigma_{np}\left(\Gamma_A^{\mu}\right)/d\omega > d\sigma_{np}\left(\Gamma_V^{\mu}\right)/d\omega > d\sigma_{nn}\left(\Gamma_V^{\mu}\right)/d\omega. \tag{A27}$$

Appendix B: Low (Soft) Energy Expansion of the $NN\nu\bar{\nu}$ Amplitudes and Characterization of the Low (Soft) Energy Region

The total neutrino-pair bremsstrahlung amplitude (M_T^μ) consists of an external amplitude (M^μ) and an internal amplitude (M_I^μ). The external amplitude is well known [see the expression of M^μ given by Eq. (6)]. However, our knowledge about the internal amplitude is somewhat limited. In the case of photon bremsstrahlung, we can impose the gauge invariant condition to determine the internal contribution, so that a conserved total amplitude can be generated.

The problem for the neutrino-pair bremsstrahlung case is that the gauge invariant condition cannot be applied to obtain an exact conserved axial vector amplitude. However, PCAC can provide an approximate conserved internal amplitude, but it is very difficult to calculate in reality. In fact, there are no existing calculations which include the PCAC contribution. In order words, all neutrino-pair bremsstrahlung calculations employ only the external amplitude for the calculation of cross sections or emissivities.

The total amplitude M_T^μ can be expanded in powers of q [the magnitude of momentum $\vec{q}$, $q^\mu = \left(\omega, \vec{q}\right)$]:

$$M_T^\mu = \frac{A_{-1}^\mu}{q} + A_0^\mu + A_1^\mu q + ... \,, \tag{B1}$$

which is called the low (soft) energy expansion of the amplitude M_T^μ. The most important difference between the external amplitude M^μ and the internal amplitude M_I^μ is that the amplitude M^μ contributes to all coefficients $\left(A_{-1}^\mu, A_0^\mu, A_1^\mu, ...\right)$, while the amplitude M_I^μ

contributes to all coefficients except the leading coefficient A_{-1}^{μ}. This fact has a significant implication. In the low (soft) energy region, the contribution from the internal amplitude M_I^{μ} (including PCAC) is expected to be insignificant or negligible, and the calculations using only the external amplitude M^{μ} should be valid. Now, the question is how to characterize the low (soft) neutrino-pair energy region. There is no standard method which can be applied to determine such a low (soft) energy region.

The main purpose of this Appendix is to introduce a method which can be applied to investigate the contribution of the leading term $\left(A_{-1}^{\mu}/q\right)$ of the expansion given by Eq. (B1) and which, by using the results of this investigation, can characterize the low (soft) energy region. More precisely, our method involves the following steps:

(1) Using Eq. (6), we obtain the amplitudes M_{pp}^{μ}, M_{nn}^{μ}, and M_{np}^{μ} for the $pp\nu\bar{\nu}$, $nn\nu\bar{\nu}$, and $np\nu\bar{\nu}$ processes, respectively.

(2) We obtain the leading terms $\left(M_{pp}^{\mu}\right)_{\ell}$, $\left(M_{nn}^{\mu}\right)_{\ell}$, and $\left(M_{np}^{\mu}\right)_{\ell}$ of the amplitudes M_{pp}^{μ}, M_{nn}^{μ}, and M_{np}^{μ}, respectively. We emphasize that these leading terms $[(M_i^{\mu})_{\ell}, (i = pp, nn, np)]$ contribute only to the leading term $\left(A_{-1}^{\mu}/q\right)$ of the expansion given by Eq. (B1).

There are at least two different ways to obtain the leading terms $\left(M_i^{\mu}\right)_{\ell}$. In addition to the one explored in Appendix A, an alternative is used in this Appendix. Here, we use the $pp\nu\bar{\nu}$ process as an example to show how the leading term $\left(M_{pp}^{\mu}\right)_{\ell}$ can be directly obtained from the expression for the amplitude M_{pp}^{μ} given by Eq. (6). The expression for M_{pp}^{μ} is a sum of four

individual external amplitudes, representing the neutrin-pair bremsstrahlung emission from two incoming proton legs and two outgoing legs. Each individual external amplitude has a denominator and a numerator. The denominator involves a $p_i \cdot q$ term $(i = 1,2,3,4)$ and a q^2 term, while the numerator involves some q-dependent terms and other q-independent terms. The leading term $\left(M^{\mu}_{pp}\right)_{\ell}$ can be obtained by the following procedure: (i) In all four denominators of M^{μ}_{pp}, we keep only the $p_i \cdot q$ term and neglect (setting to zero) the q^2 term; (ii) In all four numerators of M^{μ}_{pp}, we keep only all those q-independent terms and neglect (setting to zero) all q-dependent terms. In this way we obtain the expression of $\left(M^{\mu}_{pp}\right)_{\ell}$. Obviously, this resulting term $\left(M^{\mu}_{pp}\right)_{\ell}$ can contribute only to the leading term $\left(A^{\mu}_{-1}/q\right)$ of the expansion given by Eq. (B1).

It is easy to check that those results obtained in Appendix A [such as $\left(M^{\mu}_{vpp}\right)_{\ell}$ given in Eq. (A5) and $\left(M^{\mu}_{App}\right)_{\ell}$ given by Eq. (A9)] can be reproduced from the expression for $\left(M^{\mu}_{pp}\right)_{\ell}$.

We should also point out another advantage of using the leading term $\left(M^{\mu}_{pp}\right)_{\ell}$. This leading term yields the following two different amplitudes (both of them depend on the axial vector vertex function Γ^{μ}_{A}): (A) the first one is the plus-type amplitude $\left(M^{\mu}_{App}\right)_{\ell}$ given by Eq. (A9). The cross section $\left(\frac{d\sigma_{pp}}{d\omega}\right)_{\ell}$ is completely dominated by this plus-type amplitude. (B) The

second one is the minus-type amplitude, which is not discussed in Appendix A. This minus-type amplitude makes a minor (almost negligible) contribution to the cross section $\left(\frac{d\sigma_{pp}}{d\omega}\right)_{\ell}$.

(3) The cross sections $\frac{d\sigma_{pp}}{d\omega}$, $\frac{d\sigma_{nn}}{d\omega}$, and $\frac{d\sigma_{np}}{d\omega}$ are calculated using the amplitudes M^{μ}_{pp}, M^{μ}_{nn}, and M^{μ}_{np}, respectively, at $P = 250$ MeV/c for $\omega = 1$, 10, 25, 50, 60, and 65.3 MeV. Note that $\omega = 65.3$ MeV is the maximum kinematically allowed energy for $P = 250$ Mev/c.

(4) The cross sections $\left(\frac{d\sigma_{pp}}{d\omega}\right)_{\ell}$, $\left(\frac{d\sigma_{nn}}{d\omega}\right)_{\ell}$, and $\left(\frac{d\sigma_{np}}{d\omega}\right)_{\ell}$ are calculated using the leading terms $\left(M^{\mu}_{pp}\right)_{\ell}$, $\left(M^{\mu}_{nn}\right)_{\ell}$, and $\left(M^{\mu}_{np}\right)_{\ell}$, respectively, at $P = 250$ Mev/c for $\omega = 1$, 10, 25, 50, 60, 65.3 MeV.

The leading term $\left(M^{\mu}_{pp}\right)_{\ell}$ includes the leading term $\left(M^{\mu}_{vpp}\right)_{\ell}$ and the leading term $\left(M^{\mu}_{App}\right)_{\ell}$. The cross section $\left(\frac{d\sigma_{pp}}{d\omega}\right)_{\ell}$, which is calculated from the leading term $\left(M^{\mu}_{pp}\right)_{\ell}$, is completely dominated by the leading term $\left(M^{\mu}_{App}\right)_{\ell}$. This implies that the contribution from the term $\left(M^{\mu}_{vpp}\right)^{*}_{\ell}\ \left(M_{vpp,\mu}\right)_{\ell}$ is completely negligible. However, we emphasize that the interference terms, $\left[\left(M^{\mu}_{vpp}\right)^{*}_{\ell}\left(M_{App,\mu}\right)_{\ell} + \left(M^{\mu}_{App}\right)^{*}_{\ell}\left(M_{vpp,\mu}\right)_{\ell}\right]$, are not negligible.

(5) The percent deviations $D_i (i = pp, nn, np)$ are calculated,

$$D_i = \frac{1}{\dfrac{d\sigma_i}{d\omega}} \left| \left(\frac{d\sigma_i}{d\omega} \right)_\ell - \frac{d\sigma_i}{d\omega} \right| \times 100\% \,. \tag{B2}$$

The results are shown in Table 3.

Some important results of our investigation can be summarized as follows:

(i) As shown in Table 3, at $\omega = 25$ MeV, the calculated values of the percent deviation are 1.4% for both the $ppv\bar{v}$ and the $nnv\bar{v}$ processes, and 4.4% for the $npv\bar{v}$ process. All values are less than 5%. Moreover, in the energy region where $\omega \leq$ 25 MeV, our detailed analysis indicates that the calculated cross sections for all three $NNv\bar{v}$ processes are completely dominated by the leading term $\left(A^\mu_{-1} / q \right)$ of the expansion Eq. (B1) [i.e., the leading term $\left(M^\mu_i \right)_\ell$ $(i = pp, nn, np)$ of the external amplitude $\left(M^\mu_i \right)$ given by Eq. (6)]. We have also found that the leading term $\left(A^\mu_{-1} / q \right)$, in turn, is dominated by the axial vector component $\left(\Gamma^\mu_A \right)$ of the vertex function Γ^μ.

(ii) At $\omega = 50$ MeV, the calculated values of the percent deviation are 2.1% for the $ppv\bar{v}$ process, 2.0% for the $nnv\bar{v}$ process, and 6.2% for the $npv\bar{v}$ process. All values are less than 7%. Again, the calculated cross sections for all three processes are dominated by the leading term $\left(A^\mu_{-1} / q \right)$.

(iii) The calculated values of the percent deviation for all three $NNv\bar{v}$ processes start increasing around $\omega = 60$ MeV and reach their maximum values (19.2%, 19.1%, and 37.4% for $ppv\bar{v}$, $nnv\bar{v}$, and $npv\bar{v}$, respectively) at $\omega = 65.3$ MeV. In other words in the energy region

where $\omega \geq$ 60 MeV, the contribution from the higher order terms [$0\left(A_0^\mu\right)$] of Eq. (B1) becomes significant.

From the results summarized above, we can now discuss the characterization of the low (soft) energy region. If we set 5% to be the maximum limit of the percent deviation for the low (soft) energy region, then the low (soft) energy region will be $\omega \leq 25$ MeV. On the other hand, if we choose the maximum limit to be 7%, then the low (soft) energy region will become $\omega \leq$ 50 MeV.

Finally, it is very important to remember that our results are based on only the external amplitude, without taking into account the contribution from the internal term M_I^μ. However, the following two facts are true:

(a) The internal amplitude M_I^μ does not contribute to the leading term $\left(A_{-1}^\mu / q\right)$ of the expansion given by Eq. (B1), and

(b) The calculated cross sections for all three $NN\nu\bar{\nu}$ processes are completely dominated by the leading term $\left(A_{-1}^\mu / q\right)$ of the expansion Eq. (B1) [i.e., the leading term $\left(M_i^\mu\right)_\ell$ $(i = pp, nn, np)$ of the external amplitude M_i^μ] in the low (soft) energy region ($\omega \leq 25$ MeV or $\omega \leq$ 50 MeV). Based upon (a) and (b) it seems plausible that the contribution from the internal amplitude would be negligible in the low (soft) energy region.

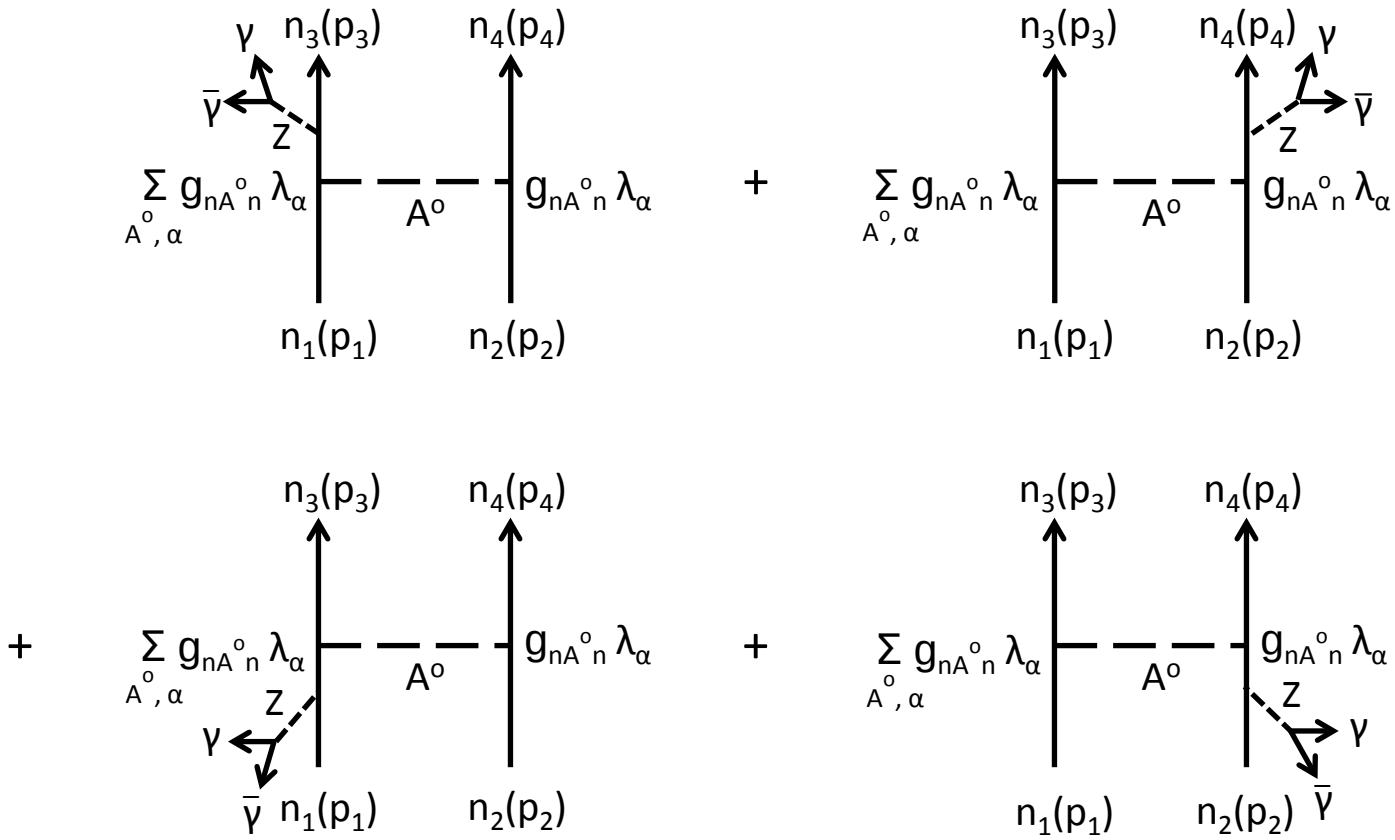

− Terms ($n_3(p_3) \leftrightarrow n_4(p_4)$)

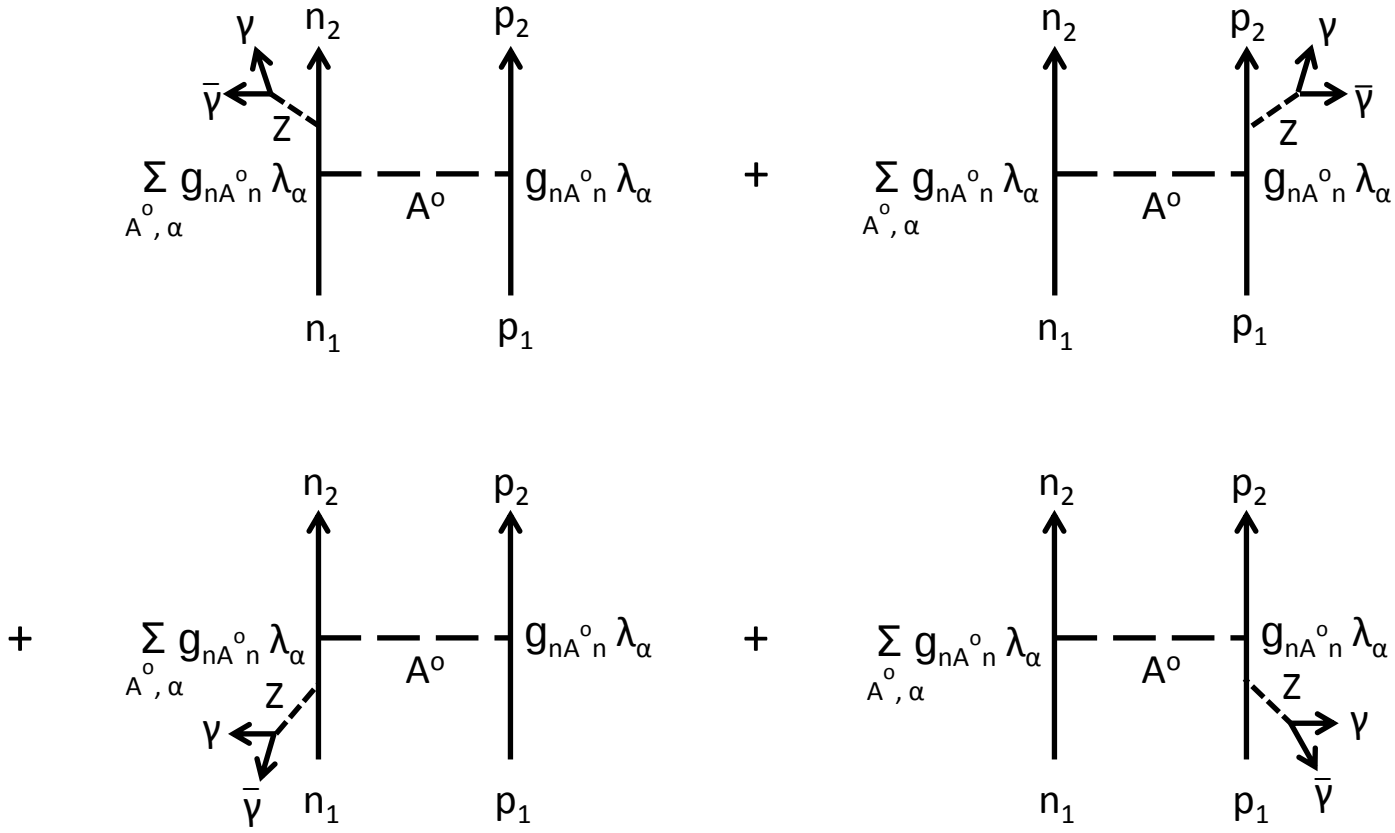
γ
n2
p2
γ̄
Z
Σ gnAonλα
Ao, α
Ao
gnAonλα
n1
p1
+
n2
p2
γ
γ̄
Z
Σ gnAonλα
Ao, α
Ao
gnAonλα
n1
p1
+
n2
p2
Σ gnAonλα
Ao, α
Z
γ
γ̄
Ao
gnAonλα
n1
p1
+
n2
p2
Σ gnAonλα
Ao, α
Ao
gnAonλα
Z
γ
γ̄
n1
p1

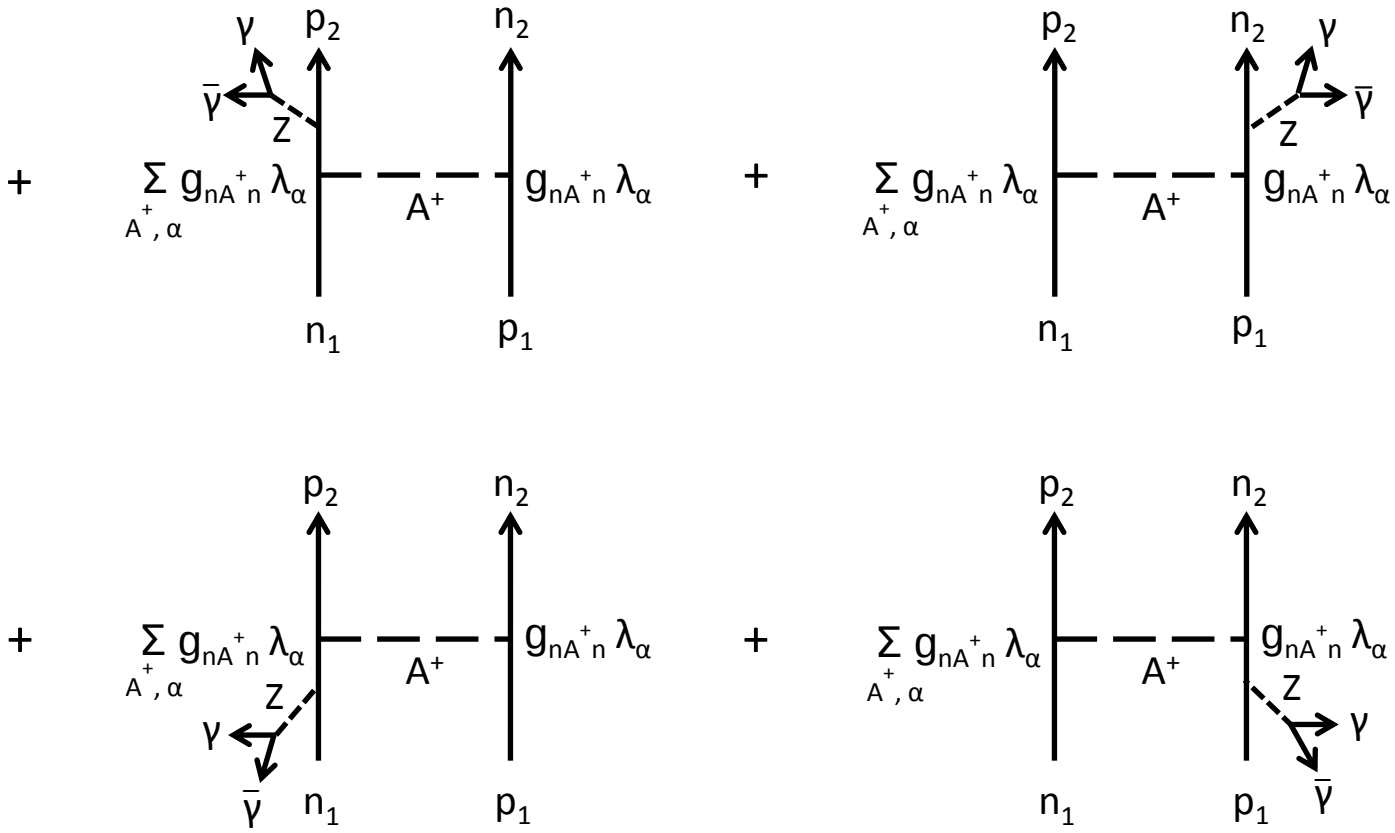
+
γ
p2
n2
γ̄
Z
Σ gnA+n λα
A+, α
A+
gnA+n λα
n1
p1
+
p2
n2
γ
Σ gnA+n λα
A+, α
Z
γ̄
A+
gnA+n λα
n1
p1
+
p2
n2
Σ gnA+n λα
A+, α
A+
gnA+n λα
Z
γ
γ̄
n1
p1
+
p2
n2
Σ gnA+n λα
A+, α
A+
gnA+n λα
Z
γ
γ̄
n1
p1

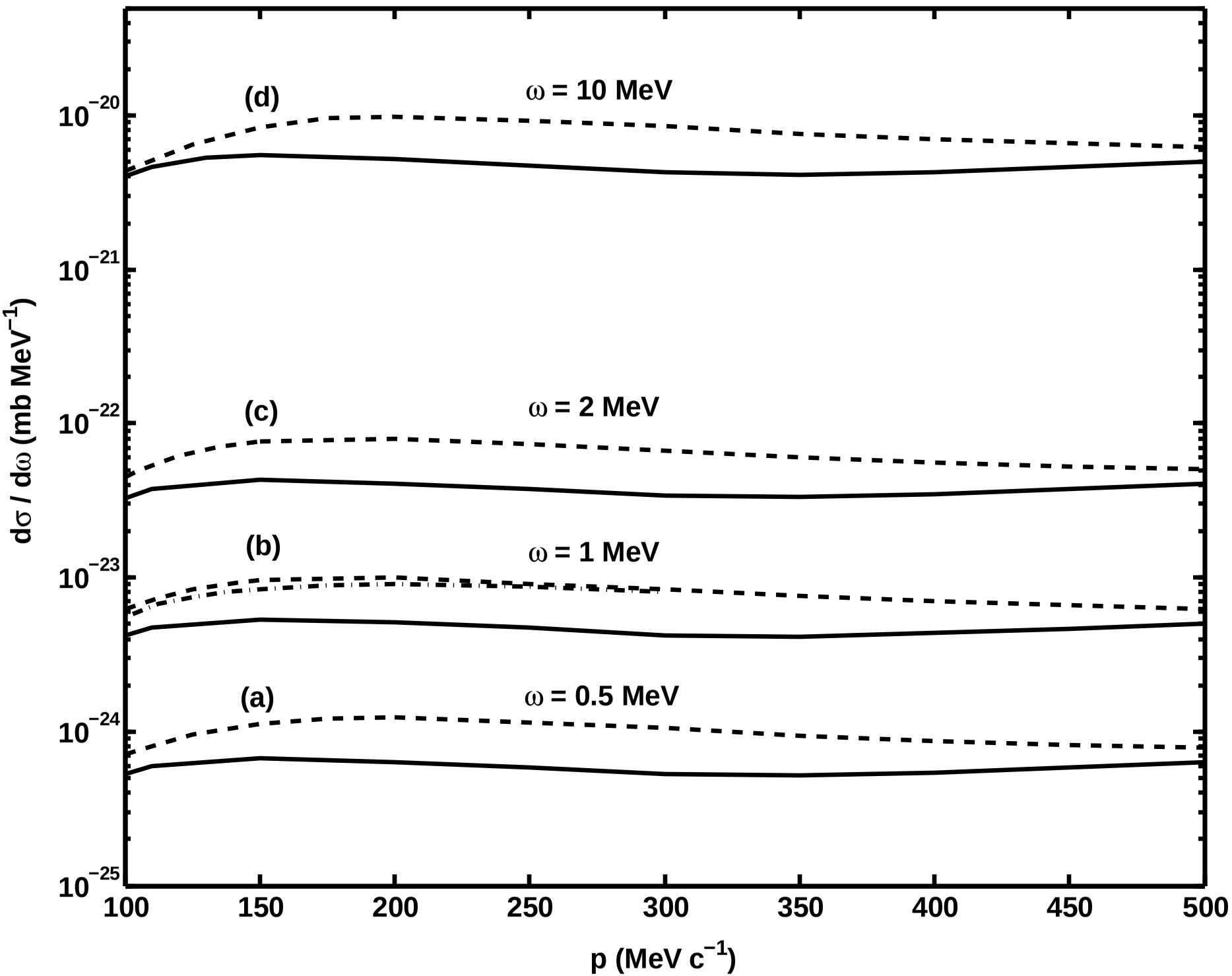
(d)
ω = 10 MeV
(c)
ω = 2 MeV
(b)
ω = 1 MeV
(a)
ω = 0.5 MeV
10^−20
10^−21
10^−22
10^−23
10^−24
10^−25
dσ / dω (mb MeV^−1)
100
150
200
250
300
350
400
450
500
p (MeV c^−1)